J. Fluid Mech. (1991), *vol.* 228, *pp.* 321–342
Printed in Great Britain

Energy spectra and coherent structures in forced two-dimensional and beta-plane turbulence

By M. E. MALTRUD[1]† AND G. K. VALLIS[2]

[1] Scripps Institution of Oceanography, La Jolla, CA 92093, USA

[2] Institute of Marine Science and Institute of Nonlinear Science, University of California, Santa Cruz, CA 95064, USA

(Received 11 June 1990 and in revised form 20 November 1990)

Results from a wide range of direct numerical simulations of forced-dissipative, differentially rotating two-dimensional turbulence are presented, in order to delineate the broad dependence of flow type on forcing parameters. For most parameter values, the energy spectra of simulations forced at low wavenumbers are markedly steeper than the classical k^{-3} enstrophy inertial-range prediction, and although k^{-3} spectra can be produced under certain circumstances, the regime is not robust, and the Kolmogorov constant is not universal unless a slight generalization is made in the phenomenology. Long-lived, coherent vortices form in many cases, accompanied by steep energy spectra and a higher than Gaussian vorticity kurtosis. With the addition of differential rotation (the β-effect), a small number of fairly distinct flow regimes are observed. Coherent vortices weaken and finally disappear as the strength of the β-effect increases, concurrent with increased anisotropy and decreased kurtosis. Even in the absence of coherent vortices and with a Gaussian value of the kurtosis, the spectra remain relatively steep, although not usually as steep as for the non-rotating cases. If anisotropy is introduced at low wavenumbers, the anisotropy is transferred to all wavenumbers in the inertial range, where the dynamics are isotropic.

For those simulations that are forced at relatively high wavenumbers, a well resolved and very robust $k^{-\frac{5}{3}}$ energy inertial range is observed, and the Kolmogorov constant appears universal. The low-wavenumber extent of the reverse energy cascade is essentially limited by the β-effect, which produces an effective barrier in wavenumber space at which energy accumulates, and by frictional effects which must be introduced to achieve equilibrium. Anisotropy introduced at large scales remains largely confined to the low wavenumbers, rather than being cascaded to small scales. When there is forcing at both large and small scales (which is of relevance to the Earth's atmosphere), energy and enstrophy inertial ranges coexist, with an upscale energy transfer and downscale enstrophy transfer in the same wavenumber interval, without the need for any dissipation mechanism between forcing scales.

1. Introduction

Since the introduction of Kolmogorov's (1941) inertial-range theory of three-dimensional turbulence, there has been much interest in determining whether such

† Current address: Department of Physics, University of California, Santa Cruz, CA 95064, USA.

inertial ranges do, in fact, exist. Data from a variety of sources (beginning with the oceanic measurements of Grant, Stewart & Moilliet 1962) have largely confirmed the prediction that the inertial-range energy spectrum is proportional to $k^{-\frac{5}{3}}$ (where k is the wavenumber), with a constant spectral flux of energy directed toward small scales.

The situation is somewhat different for two-dimensional turbulence (Batchelor 1969; Kraichnan 1967), because of the conservation of vorticity on fluid parcels in inviscid flow. The twin constraints of energy and enstrophy (mean-squared vorticity) conservation lead one to postulate the dual existence of an inverse energy cascade, with the energy flux directed toward large scales, and a cascade of enstrophy toward small scales. The inertial-range prediction for the energy cascade is $k^{-\frac{5}{3}}$, as in the three-dimensional case. The forward enstrophy cascade has a predicted inertial-range spectrum proportional to k^{-3}, with logarithmic corrections due to non-local modal interactions (Kraichnan 1967).

The first reasonably high-resolution numerical investigations of two-dimensional turbulence did not yield entirely expected results, namely space-filling turbulent flow with a uniform cascade of enstrophy to small scales. Perhaps the most noticeable aspect, especially apparent in simulations of decaying two-dimensional turbulence by Fornberg (1977) and McWilliams (1984), but also evident in studies of forced–dissipative two-dimensional turbulence by, among others, Basdevant *et al.* (1981) and Legras, Santangelo & Benzi (1988), was the appearance of long-lived coherent structures. These approximately circular structures often ended up dominating the flow and introduced a type of spatial and temporal intermittency that classical inertial-range and closure theories appear not to be able to account for.

A common feature shared by most of the forced–dissipative direct numerical simulations of two-dimensional turbulence is energy spectra steeper than k^{-3} in the enstrophy inertial range, possibly (although not unequivocally) due to the presence of coherent structures. With the possible exception of some early experiments by Lilly (1972) (in which the resolution was probably too low to give accurate results), the existence of the k^{-3} range has not been confirmed by direct numerical simulations. (Decaying turbulence cannot of itself be compared directly to inertial-range predictions based on statistically stationary forced dissipative situations. Thus, although decay simulations may exhibit transient k^{-3} spectra depending on initial conditions (Santangelo, Benzi & Legras 1989), it is rather difficult to interpret such results in relation to inertial-range theory.) On the other hand, forced simulations with fairly low inertial-range resolution (Lilly 1972; Frisch & Sulem 1984; Herring & McWilliams 1985) indicate the actual existence of the $k^{-\frac{5}{3}}$ energy inertial range.

The poor comparison with enstrophy inertial-range predictions is troubling, since without a Kolmogorovian-like phenomenology to build upon, the foundations of some of the more elaborate theories of turbulence must be suspect when applied in two dimensions. Although the DIA (Direct Interaction Approximation) itself does not *a priori* assume Kolmogorovian scaling, its derivatives, such as the test field model, certainly take little account of spatial intermittency (Herring & McWilliams 1985). Renormalization group theories (at least as applied in three dimensions) generally assume some kind of Kolmogorovian scaling (Yakhot & Orszag 1986). The coherent structures provide one obvious candidate for the differences, since in both two and three dimensions intermittency (manifested by non-space-filling structures) will provide a correction to the inertial range exponent. If this is so, then simulations in which coherent structures are not manifest should presumably yield spectra closer

to k^{-3}. (On the other hand, since the observed spectra for fully three-dimensional turbulence do seem to lie close to the $-\frac{5}{3}$ prediction, corrections due to intermittency (Kolmogorov 1962) appear small in that case.)

As well as its inherent interest, two-dimensional turbulence is of much geophysical relevance. However, large-scale geophysical flows have the added complication of differential rotation: the presence of a northward gradient of the local vertical rotation rate (the β-effect) can significantly alter the characteristics of a turbulent flow. (Other important characteristics of real geophysical fluids, such as stratification, will not be addressed here.) If the β-effect is strong enough, turbulent transfers between modes are inhibited by excitation of Rossby waves, resulting in an arrest of the reverse energy cascade (Rhines 1975; Holloway & Hendershott 1977). In addition, the β-effect can destroy the emergence of circular vortices in decay simulations (McWilliams 1984; Holloway 1984), and while some vortices have been noticed in simulations of decaying and forced turbulence with β (Salmon 1982; Basdevant *et al.* 1981), this case has not been extensively studied.

In this paper, we will present a series of numerical simulations that address some of these problems. We particularly investigate the effects of differential rotation in forced–dissipative, statistically steady, flows. Differential rotation is interesting not only for its geophysical importance but because through wave radiation it provides a mechanism for the destruction of coherent vortices. Although decaying simulations perhaps present the mechanisms of turbulence (e.g. vortex merger, wave propagation) in their purest form unencumbered by external agencies, only in forced–dissipative simulations can the energy and enstrophy inertial ranges be unambiguously established. We present simulations of both the energy and enstrophy inertial ranges, confirming the existence of a $k^{-\frac{5}{3}}$ energy inertial range over a broad range of conditions, with a numerically very well-resolved inertial range. The forward enstrophy cascade is much more delicate; we show simulations with a spectral slope close to -3 with no differential rotation, as well as simulations (generally with non-zero β-effect) which have relatively steep spectra and vorticity kurtosis values that may or may not be close to Gaussian. In addition, stable coexistent inertial ranges (i.e. both energy and enstrophy) are found when forcing occurs at both high and low wavenumbers.

The outline of the paper is as follows. In §2, the numerical model is briefly described. The two sections following describe numerical experiments that are forced at low wavenumbers, allowing for the examination of enstrophy inertial-range dynamics. Section 3 discusses this case in the absence of the β-effect, while §4 deals with the $\beta \neq 0$ case. In §5, we will describe simulations similar to those in §§3 and 4, but which are forced at relatively high wavenumbers to allow for resolution of the energy inertial range. Section 6 describes simulations forced simultaneously at low and high wavenumbers. Section 7 contains discussion and conclusions.

2. The model

The model equation used in this study is the two-dimensional vorticity equation for an incompressible, homogeneous fluid on a β-plane:

$$\frac{\partial \zeta}{\partial t} + \mathrm{J}(\psi, \zeta) + \beta \frac{\partial \psi}{\partial x} = F + D, \tag{2.1}$$

where ψ is the stream function, $\zeta \equiv \nabla^2 \psi$ is the relative vorticity, β is the northward

gradient of the Coriolis parameter, F and D represent forcing and dissipation, respectively, and J is the two-dimensional Jacobian operator:

$$\mathrm{J}(\psi, \zeta) \equiv \frac{\partial \psi}{\partial x}\frac{\partial \zeta}{\partial y} - \frac{\partial \psi}{\partial y}\frac{\partial \zeta}{\partial x}. \tag{2.2}$$

For a doubly periodic domain, we may express the vorticity and stream function in terms of a complex Fourier series, e.g.

$$\psi(x, y) \equiv \sum_{k=1}^{k_{\max}} \psi_{\boldsymbol{k}}(t)\, \mathrm{e}^{\mathrm{i}\boldsymbol{k}\cdot\boldsymbol{x}} \tag{2.3}$$

where $\psi_{\boldsymbol{k}}^* = \psi_{-\boldsymbol{k}}$ to ensure reality of the physical field. Then the equation of motion takes the following form:

$$\dot{\zeta}_{\boldsymbol{k}} + J_{\boldsymbol{k}} + \mathrm{i}k_x \beta = F_{\boldsymbol{k}} + D_{\boldsymbol{k}}, \tag{2.4}$$

where $J_{\boldsymbol{k}} = \Sigma_{pq}\, a_{\boldsymbol{k}pq}\, \zeta_p\, \zeta_q$ and $a_{\boldsymbol{k}pq}$ are certain coefficients, whose precise form does not concern us, which vanish unless $\boldsymbol{k}$, $\boldsymbol{p}$ and $\boldsymbol{q}$ form a vector triad. The nonlinear term in (2.4) is solved using the staggered grid algorithm of Patterson & Orszag (1971) with full dealiasing. Timestepping is done using the leapfrog method with a weak Robert filter applied every timestep to eliminate the computational mode and with the dissipation term lagged by one timestep for numerical stability. Most of the numerical experiments that we will describe have a maximum wavenumber $k_{\max} = 128$ or $k_{\max} = 256$, resulting in equivalent grid point resolution of 256^2 and 512^2, respectively. The resolution chosen, although not the highest achievable using current computers, enables a broad parameter regime to be explored with computer (and human) resources that are not prohibitive.

The dissipation function, D, is modelled using a high-order 'diffusion' (or scale selective filter) to dissipate the enstrophy that accumulates at the smallest resolved scales, and a linear drag to dispose of the energy that builds up at the largest scales:

$$D \equiv \alpha \nabla^2 \psi + \nu_n \nabla^{2n} \psi. \tag{2.5}$$

Simulations were performed using a conventional viscosity, for which $n = 2$, a biharmonic friction, for which $n = 3$, and a 'hyperviscosity' or 'superviscosity', for which n may be as high as 9, with few qualitative differences. We have also used the anticipated potential vorticity parameterization (Sadourny & Basdevant 1985; Vallis & Hua 1988). The advantages of higher-order viscosities are well known and lie in the higher effective Reynolds numbers achievable because dissipation is much more scale selective. Nevertheless, some simulations were carried out with a conventional viscosity as a check that the results obtained are not artifactual. The value of the diffusion coefficient, ν_n, is calculated every few timesteps during the simulation using the inverse r.m.s. vorticity as a timescale and $1/k_{\max}$ for a lengthscale, e.g.

$$\nu_n = \gamma \frac{\zeta_{\mathrm{rms}}}{k_{\max}^{2n-2}}, \tag{2.6}$$

where γ is a tuning factor typically of the order of unity. This is rather similar to using a Smagorinsky viscosity (Smagorinsky 1963). The linear drag coefficient, α, is held constant through some range of low wavenumbers (beginning at the lowest wavenumber), then is set to zero for all wavenumbers above an arbitrary cutoff and

thus has no direct influence in the simulated inertial ranges. Both the value of α and the cutoff wavenumber remain constant during any given experiment, but are variable from run to run.

For the forcing function, F, a random Markovian formulation is used:

$$F_n \equiv \hat{A}(1-R^2)^{\frac{1}{2}}e^{i\theta}+RF_{n-1}, \tag{2.7}$$

where θ is a random number in $[0, 2\pi]$, $\hat{A}$ is the (wavenumber-dependent) forcing amplitude, and the subscript on F denotes the timestep. R is a function of the timestep and the forcing correlation time (t_f), being equal to zero for white noise and increasing to unity for infinite correlation time. The forcing is applied to all wavenumbers (with a different value of θ for each) whose magnitude falls into a defined range, e.g. for $10 \leqslant |\boldsymbol{k}| \leqslant 14$. This forcing range, as well as the values of t_f and $\hat{A}$ remain constant during any given experiment, but are variable from run to run.

Simulations are run until a quasi-steady state is reached that is characterized by fluctuations in the total energy and enstrophy about some well-defined mean value and when the average energy and enstrophy injection rates are approximately equal to their respective dissipation rates. At this point, the simulations are continued for an extended period to obtain robust averages.

3. Low-wavenumber forcing, isotropic cases

3.1. *Flows with coherent structures*

For a fairly wide parameter range, the vorticity field has a significant component made up of coherent vortices that are very long-lived compared with typical flow timescales, such as a large-scale advective time, or an eddy turnover time. The remainder of the field is a more typically 'turbulent' background flow (see also Basdevant *et al.* 1981, and Legras *et al.* 1988). Typical flow diagnostics show distinct variations from Gaussian inertial-range assumptions and predictions. For instance, the vorticity kurtosis (kurtosis $\equiv Ku(\zeta) \equiv \langle\zeta^4\rangle/\langle\zeta^2\rangle^2$ where $\langle\ \rangle$ denotes an area average) attains values significantly greater than the Gaussian random value of 3, indicating some degree of spatial intermittency. However, the value of the stream-function kurtosis remains in the vicinity of 3. (The appearance of coherent structures is defined subjectively. However, they are always accompanied by high values of the vorticity kurtosis.)

Coherent structures emerge under a wide range of circumstances, largely independent of the resolution (provided it is reasonably high), the forcing range, the forcing amplitude, the particular form of the enstrophy dissipation function, or the initial conditions, though the specifics of each flow will, of course, be different. However, low-wavenumber dissipation can prevent vortices from emerging in some cases, as we will see in §3.2. Figure 1(*a*) (plate 1) presents a map of the vorticity field from a typical forced experiment. Note that coherent structures are present at a range of scales, and that the scale of the strongest vortices is not determined by domain size or by the extent of the low-wavenumber dissipation range, but largely by the forcing range. We also see vortices with significant strength at scales smaller than the forcing scale, but very few larger than this scale.

Examination of the isotropic (averaged over angles in wavenumber space) energy spectra, $E(k)$, of flows that exhibit coherent structures yields two interesting observations. First, there are two somewhat distinct spectral slopes in the inertial range between the forcing and dissipation wavenumbers, with the transition between the two regimes occurring at an approximate wavenumber k_T (figure 2*a*). As

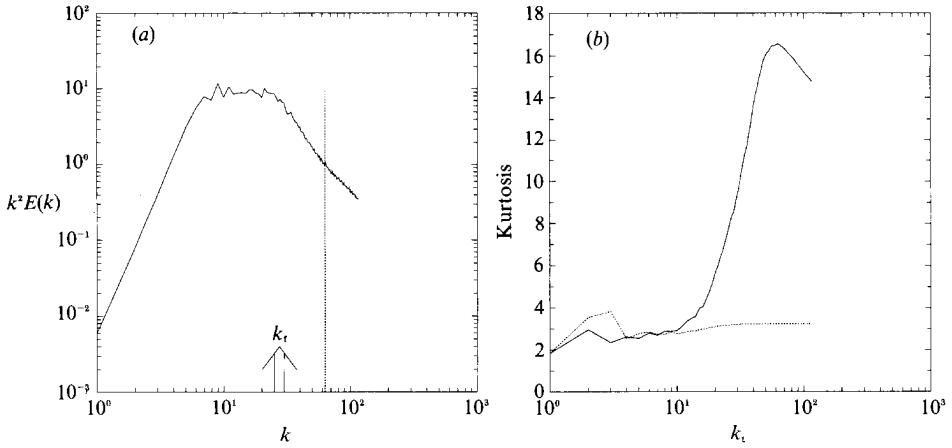

FIGURE 2. (*a*) Average enstrophy spectrum ($k^2E(k)$) from a simulation forced in the range $25 \leqslant k \leqslant 30$ (denoted by k_f). The slope of the lower-wavenumber range (approximately $30 \leqslant k \leqslant 60$) is -2.5, the slope of the higher-wavenumber range (approximately $60 \leqslant k \leqslant 110$) is -1.6. The dashed line indicates the peak ($k = 63$) in the kurtosis plot in (*b*). (*b*) The kurtosis of the vorticity field (solid curve) and stream function (dashed curve) reconstructed using only modes 1 to k_t plotted as a functionof k_t, where k_t is the truncation wavenumber defined in the text.

mentioned by Legras *et al.* (1988), the lower (smaller wavenumber), steeper range seems to be due to the presence of vortices. Figure 2(*b*) shows some support for this assertion. The vorticity field from a typical simulation is reconstructed using only those Fourier modes with wavenumber magnitude smaller than a given truncation wavenumber, k_t, which is less than or equal to the maximum wavenumber resolved by the full model, k_{max}. We can then plot the kurtosis of the reconstructed field as a function of truncation wavenumber. It is seen in figure 2(*b*) that the reconstructed field with the highest kurtosis contains only wavenumbers 1 to $k_T \approx 63$, implying that the high kurtosis of the true field is principally due to the contribution of these modes. (The reason for the decrease in kurtosis for $k > k_T$ is unknown.)

The value of k_T depends to some degree on numerical resolution, becoming larger with increasing resolution and decreasing viscosity. While k_T is not what is typically referred to as the dissipation wavenumber, it does seem to represent the range of wavenumbers for which the effect of the dissipation is somehow felt. That is, vortices of scales somewhat larger than the effective Kolmogorov scale can nevertheless feel the effects of viscosity, if indirectly. As the Kolmogorov scale increases with increasing resolution, smaller-scale vortices are allowed to evolve essentially frictionlessly, thus extending the spectral range affected by the presence of vortices. Whether k_T will continue to grow without bound as the numerical resolution gets very large is an open question.

The second characteristic of these spectra is the fact that both of the enstrophy subranges have slopes that are significantly steeper than the k^{-3} (energy spectral slope) behaviour predicted by classical inertial-range theory. In addition, the slopes that are seen depend strongly on the particular forcing parameters being used, particularly the forcing range and forcing correlation time, reflecting the strength and scale of the structures present. Corrections have been made to the inertial-range arguments to account for spatial and temporal intermittency based on the identification of subdomains of 'active' turbulence being principally responsible for the enstrophy cascade (Basdevant *et al.* 1981; Benzi *et al.* 1986), resulting in the

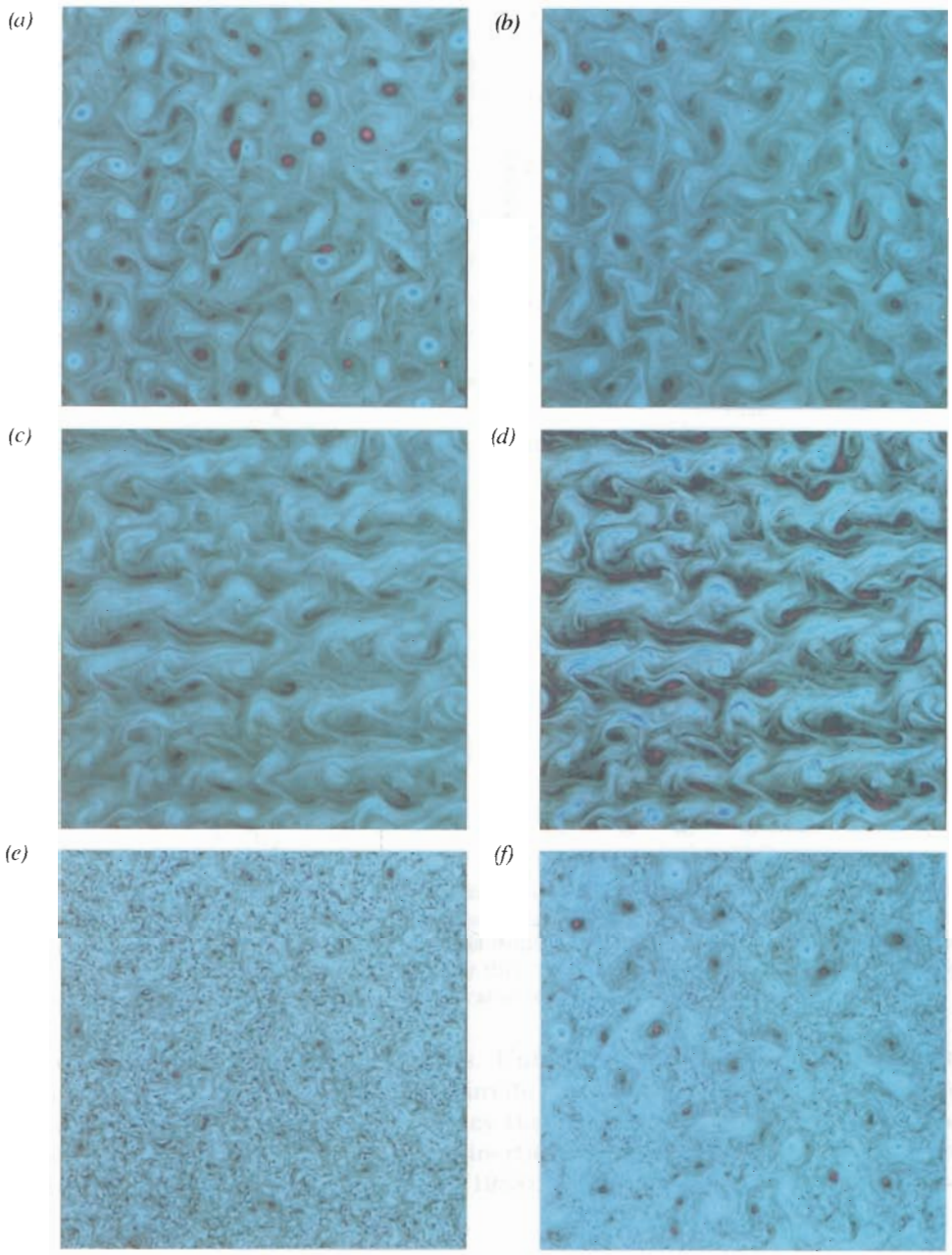

FIGURE 1. Relative vorticity from typical simulations with $k_{max}=128$. *(a)* Forced in the range $10 \leqslant k \leqslant 14$. *(b)* Forced in the range $10 \leqslant k \leqslant 14$ with $k_\beta=3.3$. All other parameters and the plotting scale are the same as in *(a)*. *(c)* Forced in the range $10 \leqslant k \leqslant 14$ with $k_\beta=4.8$. All other parameters and the plotting scale are the same as in *(a)*. *(d)* Same as *(c)* except that the plotting scale has been changed to highlight elongated flow structure. *(e)* Forced in the range $80 \leqslant k \leqslant 84$. *(f)* Forced in the range $10 \leqslant k \leqslant 14$ and $80 \leqslant k \leqslant 84$. (Although simulations similar to those shown in *(e)* and *(f)* were also performed with high-wavenumber forcing in the range $160 \leqslant k \leqslant 165$, but the forcing scale is then too small to be resolved by the eye in these figures.)

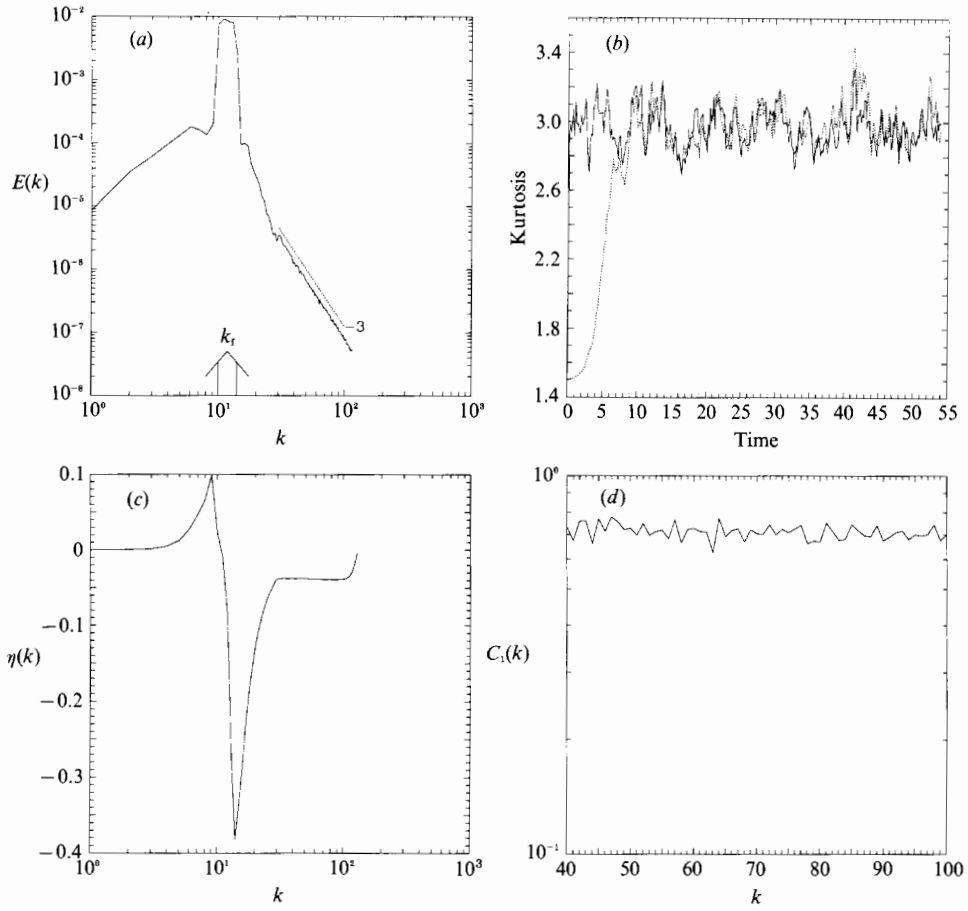

FIGURE 3. Flow diagnostics from a simulation forced in the range $10 \leqslant k \leqslant 14$ exhibiting no coherent structures with low-wavenumber dissipation acting for $k \leqslant 30$. (*a*) Time-averaged energy spectrum. (*b*) Time series of vorticity kurtosis (solid curve) and stream-function kurtosis (dashed curve). (*c*) Time-averaged spectral enstrophy flux, $\eta(k)$, as defined by (3.3). (*d*) The Kolmogorov constant $C_1(k) = k^3 E(k)\,\eta(k)^{-\frac{2}{3}}$. The average value of C_1 is 0.7.

expectation of steeper spectral slopes. Unfortunately, it is difficult to locate the active domains precisely enough to invite quantitative comparison between our numerical simulations and intermittency theories. In addition, these theories, again, predict a single spectral slope for the inertial range, in contrast to the two distinct slopes seen here and by Legras *et al.* (1988).

3.2. *Flows without coherent structures*

While most of our simulations with $\beta = 0$ exhibit coherent structures, it is possible to find circumstances where vortices apparently do not form. This is done by extending the range of the low-wavenumber dissipation up to a wavenumber that significantly exceeds the upper limit of the forcing range, although not extending into the inertial range. In addition, the forcing correlation time must be quite short, typically a small multiple of the numerical timestep. Figure 3 shows this type of simulation where dissipation destroys any structures that weakly begin to form initially, resulting in the average vorticity kurtosis being approximately the random value of 3.

The energy spectra that result from these types of flows are quite close to being proportional to k^{-3} (figure 3*a*), further supporting the general assertion that coherent structures are associated with steep spectral slopes. (However, in the next section we present some results of spectra steeper than k^{-3} with no coherent structures.) Of course, the spectral slope in the inertial range, should, according to the Kolmogorovian paradigm, not be dependent on such details as the forcing correlation timescale. The dependence of the spectral slope on such details is therefore an indication of the non-universality of that range. Given the predicted inertial-range form,

$$E(k) = C_1 \eta^{\frac{2}{3}} k^{-3}, \tag{3.1}$$

where η is the enstrophy cascade rate (and ignoring logarithmic corrections) we can solve for the universal constant C_1 by fitting our spectrum to the prediction.

From the spectral form of the equation of motion (2.4), we obtain the enstrophy equation for a single Fourier mode,

$$\frac{\partial}{\partial t}(\tfrac{1}{2}\zeta_k^2) + \zeta_k^* J_k = \zeta_k^* F_k + \zeta_k^2 \nu_n k^{2n-2} \tag{3.2}$$

and we can see that the enstrophy flux through wavenumber space is

$$Fl_\zeta(k) = Re \sum_{|l|=1}^{k} \zeta_l^* J_l \tag{3.3}$$

since $\zeta_l^* J_l$ is the divergence of this flux. The cascade rate, $\eta(k)$, is equal to the average of $Fl_\zeta(k)$ in the inertial range in a statically steady state. Figure 3(*c*) shows that the enstrophy flux is quite flat throughout the inertial range in our calculation. If C_1 is truly constant, then a plot of

$$C_1(k) = E(k)\,\eta(k)^{-\frac{2}{3}} k^3 \tag{3.4}$$

should be independent of k in the inertial range. Figure 3(*d*) exhibits this type of plot which shows that $C_1(k)$ is essentially constant, except for some noise presumably due to finite averaging. The mean value in this case is $C_1 = 0.7$, which does not compare well with the value $C_1 = 1.74$ that has been predicted by Leith & Kraichnan (1972) using the test field model closure. Additional simulations of this type have shown that the value of C_1 is somewhat sensitive to some model parameters, such as the forcing amplitude and correlation time, suggesting the importance of non-local interactions. Figure 4(*a*, *b*) shows the effect of changing the forcing correlation time (t_f) and the forcing amplitude ($\hat{A}$) on the spectral slope, and figure 4(*c*) shows the effect of these changes on the value of $C_1(k)$. (Sensitivity to forcing parameters is also seen by Basdevant *et al.* (1981), as very different structures and spectral slopes result if negative viscosity instability forcing is used instead of random stirring.)

This apparent non-universality in the k^{-3} range can be investigated by examining the derivation of (3.1), namely that the enstrophy cascade rate scales as the ratio of the enstrophy and a timescale τ, (e.g. Vallis 1985). That is

$$\eta(k) = C_1^{-\frac{3}{2}} \frac{k^3 E(k)}{\tau(k)}, \tag{3.5}$$

where the proportionality constant C_1 is chosen for consistency with (3.1). If for the eddy turnover time we use the local expression $\tau_1(k) = [k^3 E(k)]^{-\frac{1}{2}}$, then we get equation (3.1) for the spectrum and (3.4) for the Kolmogorov constant. If we chose the potentially non-local turnover time

$$\tau_2(k) = \left[\int_1^k p^2 E(p)\,\mathrm{d}p\right]^{-\frac{1}{2}} \tag{3.6}$$

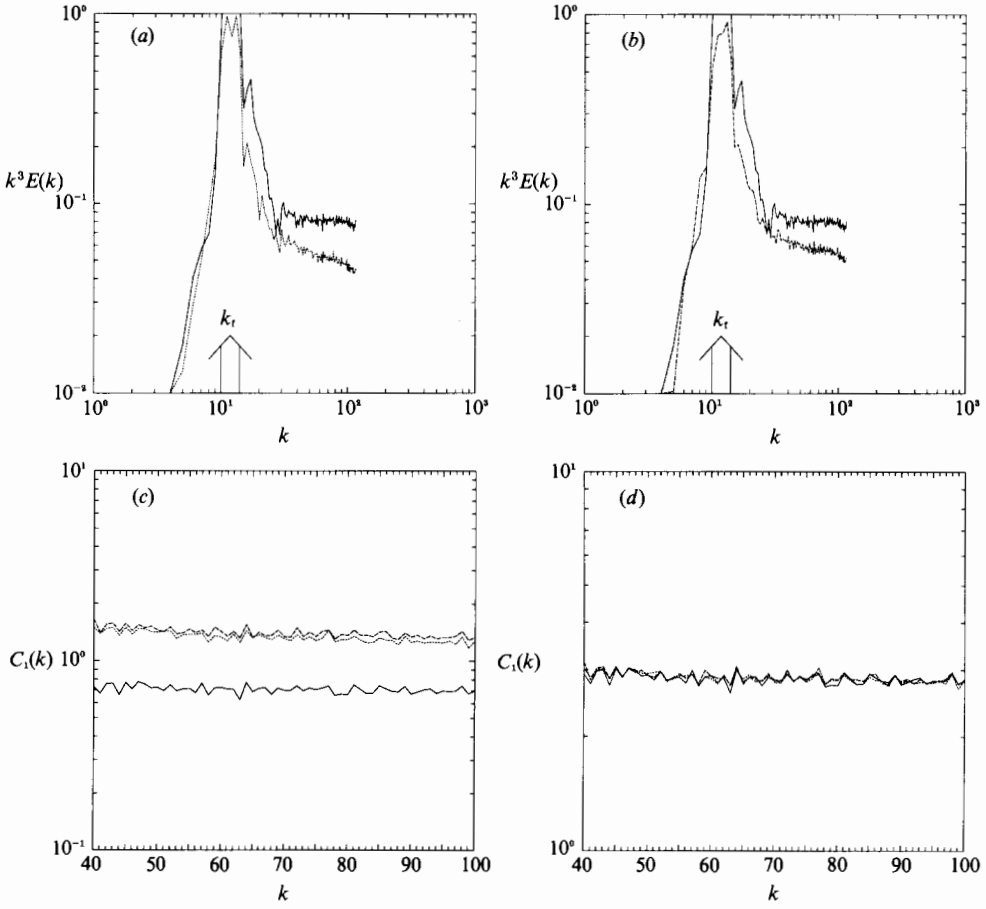

FIGURE 4. Results from simulations forced in the range $10 \leqslant k \leqslant 14$ with low-wavenumber dissipation acting for $k \leqslant 30$. (*a*) Average enstrophy spectra multiplied by k. The solid curve is the same data seen in figure 3(*a*). The dashed curve has a forcing correlation time that is 12.5 times greater and has been shifted down for clarity. (*b*) Average enstrophy spectra multiplied by k. The solid curve is the same as in (*a*). The dashed curve has a forcing amplitude that is 4 times greater and has been shifted down for clarity. (*c*) The Kolmogorov constant $C_1(k) = [\eta(k)\tau(k)/k^3E(k)]^{-\frac{2}{3}}$, where $\tau(k) = [k^3E(k)]^{-\frac{1}{2}}$. The average value of the solid curve (corresponding to the solid spectrum in *a* and *b*) is 0.7. The average value of the short-dashed curve (corresponding to the dashed spectrum in *a*) is 1.3. The average value of the long-dashed curve (corresponding to the dashed spectrum in *b*) is 1.4. (*d*) The modified Kolmogorov constant $C_1(k) = [\eta(k)\tau(k)/k^3E(k)]^{-\frac{2}{3}}$, where $\tau(k) = [\int_1^k p^2E(p)\,\mathrm{d}p]^{-\frac{1}{2}}$ for the same cases as in (*c*). The average value of all of the curves is 2.9. (The apparent correlation in the curves is due to the particular algorithm used for calculating isotropic spectra.)

(used in deriving the log-corrected spectrum $E(k) \sim \eta^{\frac{2}{3}}k^{-3}(\log k/k_0)^{\frac{1}{3}}$ by Kraichnan 1967), we obtain the expression

$$C_1(k) = \eta(k)^{-\frac{2}{3}}k^2E(k)^{\frac{2}{3}}\tau_2(k)^{-\frac{2}{3}}. \tag{3.7}$$

as a modified Kolmogorov constant. This expression actually yields much more universal behaviour. Figure 4(*d*) shows that the values of $C_1(k)$ are almost identical to each other when we use $\tau_2(k)$ (as calculated from the model spectra) in (3.7) for the same model integrations as seen in figure 4(*c*).

Since the energy spectrum is strongly peaked in the forcing range in this class of simulations, the integral in the definition of τ_2 is dominated by contributions from wavenumbers in the vicinity of k_f, so τ_2 is constant in the inertial range. This implies a non-local interaction in k-space, with the large scales directly straining much smaller scales. Hence we would not necessarily expect the Kolmogorov constant C_1 (based on a hypothesis of local interactions in k-space) to be universal under these conditions. The fact that we do see some kind of universality here is reminiscent of a large-scale straining occurring in passive-scalar advection, as discussed in Holloway & Kristmannsson (1984), Lesieur & Herring (1985), and Babiano *et al.* (1987), implying that the small-scale vorticity is here behaving as a passive scalar.

4. Low-wavenumber forcing with anisotropy

The addition of a finite value of β to simulations similar to those described above can alter the flow to varying degrees, depending on its strength. We measure this strength by defining a wavenumber, k_β, at which the nonlinear term in the equation of motion ($\mathrm{J}(\psi, \zeta)$) is of the same order as the Rossby-wave propagation term ($\beta\partial\psi/\partial x$). k_β then represents the approximate location of a transition zone between turbulent and wavelike regimes. The particular choice of the flow timescale in this scaling process can result in different definitions for k_β. If we suppose that k_β lies at the lower-wavenumber end of a reverse energy cascade, then it is sensible to scale k_β in terms of the energy cascade rate ϵ and β, yielding

$$k_\beta \sim \left(\frac{\beta^3}{\epsilon}\right)^{\frac{1}{5}}. \tag{4.1}$$

Similarly, using the enstrophy cascade rate η gives

$$k_\beta \sim \frac{\beta}{\eta^{\frac{1}{3}}}. \tag{4.2}$$

However, the physical circumstance when (4.2) would be appropriate is not as clear. If the energy is concentrated near k_β, then we can eliminate ϵ in favour of the mean energy U^2 using the dimensionally correct substitution $U^2 \sim \epsilon^{\frac{2}{3}} k_\beta^{-\frac{2}{3}}$. We then recover Rhines' (1975) expression

$$k_\beta^{\mathrm{R}} \sim \left(\frac{\beta}{2U}\right)^{\frac{1}{2}}. \tag{4.3}$$

(The factor of 2 in the denominator is a little arbitrary here.) The expression of Holloway & Hendershott (1977) can similarly be recovered from (4.2), namely

$$k_\beta^{\mathrm{H}} \sim \frac{\gamma}{\zeta_{\mathrm{rms}}}, \tag{4.4}$$

where ζ_{rms} is the root-mean-square vorticity, as well as by independent reasoning given therein. For most of our simulations we are concerned with rather small values of k_β, which do not extend into the enstrophy range, and thus (4.1) is appropriate. Since a reverse energy cascade rate is not always resolved, we find it simpler just to calculate (4.3). Using k_β^{H} was found to make no qualitative difference in our cases.

Beta has two somewhat distinct effects on the flow. One is to inhibit the reverse cascade of energy to large scales, by the scattering of 'turbulent' energy to 'wave' energy, the transition occurring approximately at k_β. The second is to introduce

anisotropy. Indeed, if the β-effect is sufficiently strong, a possible end state for decaying turbulent flows on the β-plane is one of alternating zonal (east–west) jets (Rhines 1975). Scaling arguments suggest that the direct effects of β in inducing anisotropy are confined to wavenumbers of less than or order k_β, although the anisotropy may persist at higher wavenumbers through nonlinear effects (Holloway & Hendershott 1977; Basdevant *et al.* 1981).

4.1 *Flow regimes*

We can divide our simulated flows on the β-plane into three fairly well-defined regimes based on the values of two flow diagnostics. One of these is the vorticity kurtosis which, again, is a gross measure of spatial intermittency and an indicator for the presence of coherent vortices. The second diagnostic is the average anisotropy of the flow, defined as $(\langle u^2\rangle - \langle v^2\rangle)/(\langle u^2\rangle + \langle v^2\rangle)$, where u and v are the zonal (east–west) and meridional (north–south) velocities, respectively, and $\langle\ \rangle$ denotes an area average.

The first flow regime occurs when k_β is less than a value of approximately unity. In this case the flow is close to being indistinguishable from the $\beta = 0$ case, based on kurtosis and anisotropy values, as well as energy spectra and examination of maps of the vorticity and stream-function fields. This result agrees with Holloway's (1984) decay experiments in that β is important in these types of simulations if the longest resolved waves can feel its presence, independent of the location of the spectral peak.

As the value of k_β is increased above unity the vorticity kurtosis drops sharply while the anisotropy remains low. The drop in kurtosis results from a reduction in the strength of the vortices relative to the background due to the β-effect actively radiating away vortex energy as Rossby waves. Even so, circular vortices are still recognizable in maps of vorticity (figure 1*b*) (plate 1), and seem to be opposing the flow's tendency to become anisotropic. The strongest vortices are now seen at slightly smaller scales than for $\beta = 0$, and are fewer in number. Though some larger-scale vortices may still be detected, their strengths have been substantially reduced.

When k_β is increased further, the anisotropy of the flow increases rapidly while the vorticity kurtosis levels off at a value of around 3, indicating the existence of few (if any) coherent vortices. Examination of the vorticity and stream-function fields shows substantially fewer vortices than in the previous regimes. Those vortices that are present are substantially smaller and are superimposed on a noticeably non-isotropic background flow (figure 1*c*, *d*) (plate 1). Vortices become ever weaker, sparse and smaller in scale as k_β increases toward the forcing range.

The boundaries between the three flow regimes are not sharply defined, i.e. the transition can occur over a range of a few wavenumbers. In addition, each boundary varies its position depending on the particular forcing and dissipation parameters chosen for a given set of experiments, with the exception of the lowest transition which always occurs near $k_\beta = 1$. The characteristics and wavenumber range of each flow regime can be seen in figure 5, where kurtosis and anisotropy are plotted as functions of k_β for two different sets of experiments.

4.2 *Energy spectra*

Although flows with $\beta \neq 0$ may become anisotropic, the isotropic energy spectrum (i.e. averaged over angles in wavenumber space) is still a useful tool. To a rough degree, the three flow regimes described above are reflected in the energy spectra. As mentioned above, energy spectra for $k_\beta < 1$ are hard to distinguish from those with $k_\beta = 0$, with dual spectral slopes for flows with coherent structures. As k_β increases

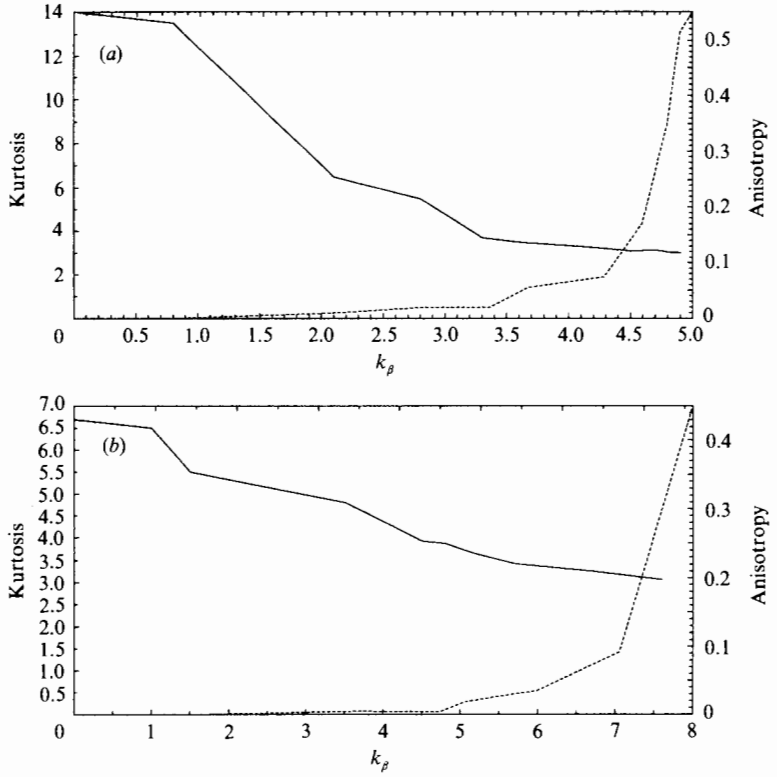

FIGURE 5. Average vorticity kurtosis (solid curve) and the average anisotropy (dashed curve) as functions of k_β define the three flow regimes described in the text. (*a*) The system is forced in the range $10 \leqslant k \leqslant 14$ with low-wavenumber dissipation acting for $k \leqslant 6$. (*b*) The system is forced in the range $25 \leqslant k \leqslant 30$ with low-wavenumber dissipation acting for $k \leqslant 10$.

above unity, the steeper, lower-wavenumber spectral range shallows as the vorticity kurtosis drops, further indicating that coherent vortices are responsible for steep slopes. The shallowing of the slope continues until it nears the slope of the higher-wavenumber range, which does not change in this regime. This regime seems to be similar to the 'clipping' scheme used by Babiano *et al.* (1987), wherein all vortices had their amplitude artificially clipped down to some constant low value, resulting in a spectrum that approached k^{-3} as the arbitrary clipping value decreased. It differs from the addition of the β-effect in that our dynamical clipping mechanism is now scale dependent, so we instead get a spectrum that approaches a uniform slope throughout the inertial range, yet remains steeper than k^{-3} (figure 6*a*).

When the system moves to the third flow regime (characterized by high anisotropy), the inertial-range spectral exponent (by now uniform) takes a value that is typically about halfway between -3 and -4 (figure 6*b*). The spectrum may either shallow with respect to the spectrum in the second regime, as in figure 6(*b*), or steepen, depending on the slope of the spectrum in the second regime. The anisotropy of the flow is especially apparent if we examine the spectra of zonal and meridional motions separately (figure 7*a*). The appearance of anisotropy at wavenumbers smaller than k_β is directly predicted by weakly nonlinear analysis theory (Rhines 1975); it is essentially a consequence of the flow seeking both a large scale (by the upscale energy cascade) and a low frequency (by a wave instability mechanism).

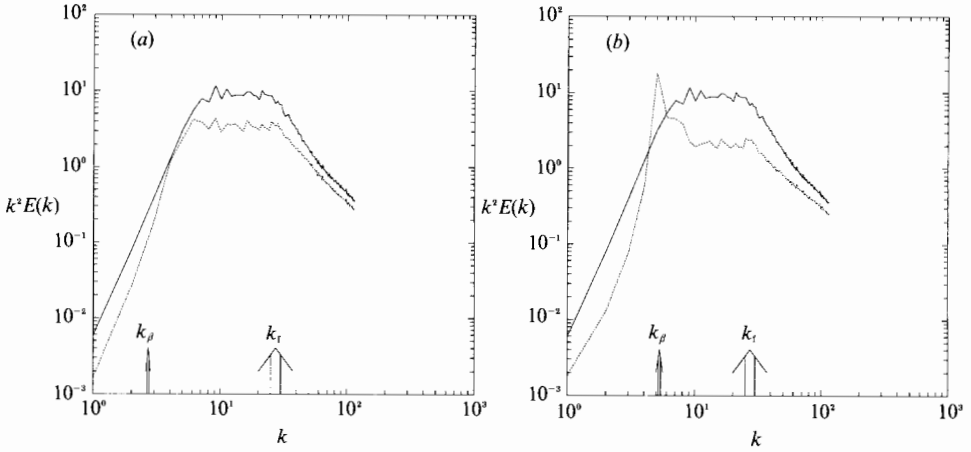

FIGURE 6. Average enstrophy spectra from simulations forced in the range $25 \leqslant k \leqslant 30$ with low-wavenumber dissipation acting for $k \leqslant 10$. (*a*) Spectra for $k_\beta = 0$ (solid curve) and for $k_\beta = 2.7$ (dashed curve). The dashed curve has been shifted down for clarity. (*b*) Spectra for $k_\beta = 0$ (solid curve) and for $k_\beta = 5.3$ (dashed curve). The slope of the dashed curve in the inertial range is approximately -1.4, and has been shifted down for clarity. Note the buildup of energy near k_β in the dashed curve.

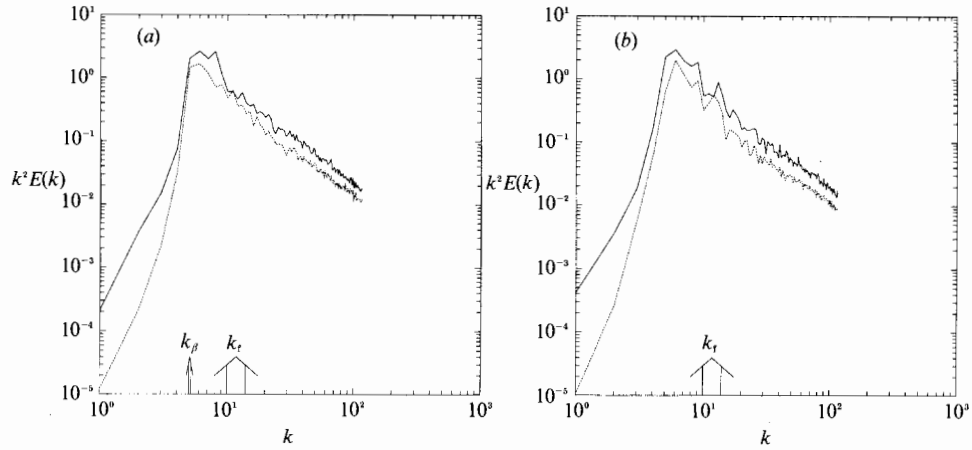

FIGURE 7. Enstrophy spectra of zonal motions (solid curve) and meridional motions (dashed curve) from simulations forced in the range $10 \leqslant k \leqslant 14$. (*a*) True β-effect with $k_\beta = 5.1$. (*b*) Anisotropic forcing with $\beta \neq 0$ for $k \leqslant 14$. Otherwise, this case uses the same parameters as in (*a*).

However, the origin of the small-scale anisotropy is less obvious, because a simple scaling of the relative magnitudes of the β-effect and the nonlinear terms (such as that done at the beginning of this section) implies that the β-effect should not be directly important in the inertial range. In our simulations the anisotropy is largely constant in the inertial range (i.e. both spectra have the same slope). Similar results are to be found in the closure-model calculations of anisotropic turbulence by Herring (1975) and of β-plane turbulence by Holloway & Hendershott (1977).

To investigate the origin of the inertial-range anisotropy, we introduced an anisotropic forcing at low wavenumbers to the system, while keeping the dynamics in the inertial-range scales strictly isotropic. This is actually done by allowing the β-effect to be non-zero only at low wavenumbers, setting its value in (2.4) to zero for all k above the forcing scales, thereby eliminating the possibility of the anisotropy

being generated at those wavenumbers by the direct influence of an anisotropic term in the equations of motion. The system can now be thought of as non-rotating two-dimensional turbulence with a non-isotropic forcing confined to low wavenumbers. The energy spectra that result from such a calculation (figure 7*b*) maintain their anisotropy at all scales, and show that the inertial-range anisotropy seen in simulations with the true β-effect (figure 7*a*) is not due to the direct action of β at those scales. Instead, plots of the vorticity field (figure 1*c*, *d*) seem to show long east–west filaments formed directly by large-scale anisotropic straining, implying that the anisotropy is non-locally transferred to the smaller scales. This interpretation agrees with closure theories of anisotropic turbulence (Herring 1975; Holloway & Hendershott 1977) which predict production of anisotropy at small scales due to large-scale straining which competes with the tendency for a return to isotropy among small-scale interactions. The former effect evidently dominates in these simulations.

We may also add β to those simulations which in the absence of β produces spectra approximately proportional to k^{-3}. In this case, the spectrum steepens until the slope reaches a value approximately halfway between -3 and -4, just as in the above case. Unfortunately, these experiments are dominated by bottom friction to such an extent that it is difficult to determine how the small amount of anisotropy that is present gets distributed among the different flow scales. However, if the mechanism for transfer of anisotropy is non-local straining, it is reasonable to suspect that anisotropy is likely to be present at all scales in the inertial range, as in the above cases.

5. High-wavenumber forcing

In this section, we examine the inverse cascade of energy to small wavenumbers. To maximize the extent of the possible inertial range, the forcing range is placed as near as possible to the maximum resolved wavenumber, for example, $F_{\boldsymbol{k}} \neq 0$ for $80 \leqslant |\boldsymbol{k}| \leqslant 84$ for $k_{\max} = 128$, while still allowing a small enstrophy range at higher wavenumbers. This also minimizes the effect of the low-wavenumber energy dissipation range on the inertial-range dynamics.

5.1 *Isotropic flows*

Just as in our simulations forced at low wavenumbers, coherent structures form at the forcing scale and values of the vorticity kurtosis greater than 3 are found (figure 8*b*), though the values are smaller than for the low-wavenumber experiments. This is probably due to the close proximity of the forcing range to the dissipation range, resulting in fewer, less strong vortices. Further, there is no evidence that the cascade of energy to larger scales produces vortices at scales much larger than the forcing scale (figure 1*e*) (plate 1).

Typically, most of our simulations have energy spectra that are slightly steeper than the inertial-range prediction,

$$E(k) = C_2 \epsilon^{\frac{2}{3}} k^{-\frac{5}{3}}, \tag{5.1}$$

where ϵ is the energy cascade rate (figure 8*a*). However, the differences in slope are so small that is possible to estimate a value for C_2. We can determine ϵ in a manner identical to that used to find the enstrophy cascade rate, using the calculated spectral energy fluxes ($Re\, \Sigma_{|l|=1}^{k} \psi_l^* J_l$). Figure 8(*d*) shows a plot of $C_2(k) = E(k)\, \epsilon(k)^{-\frac{2}{3}} k^{\frac{5}{3}}$ which again has a fairly well-defined mean ($C_2 = 5.8$) with some superimposed noise.

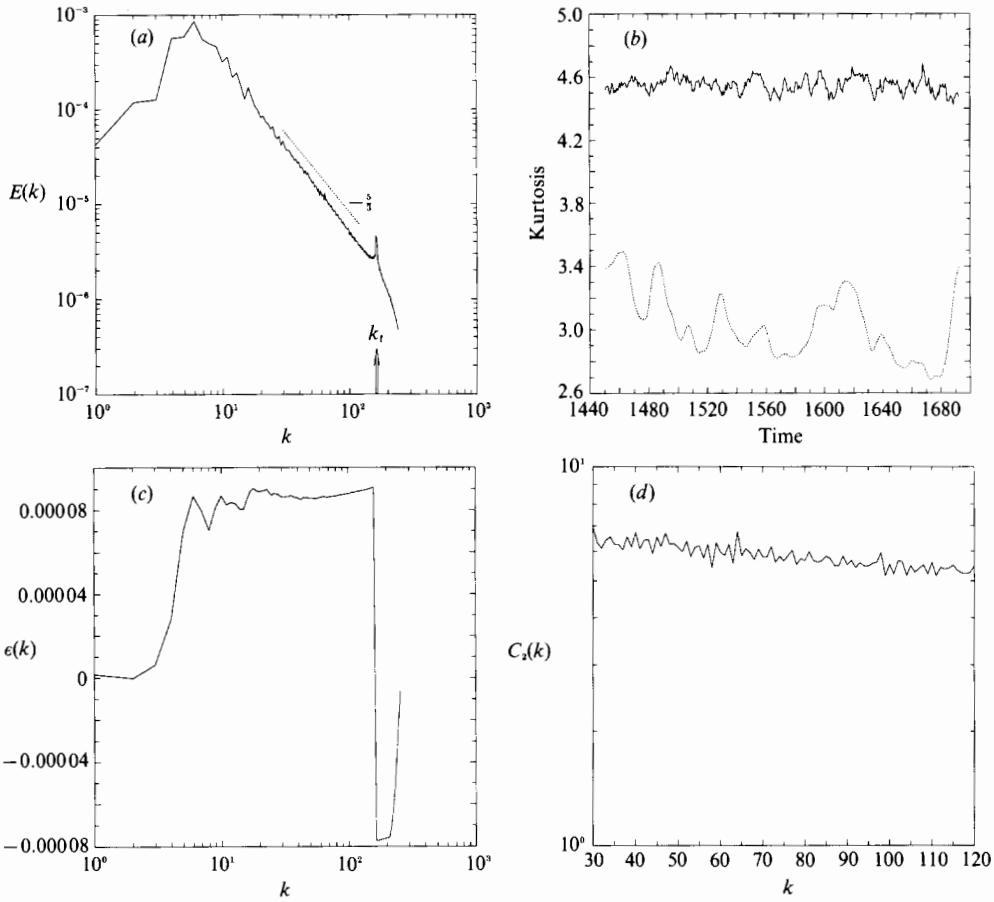

FIGURE 8. Flow diagnostics from a simulation forced in the range $160 \leqslant k \leqslant 165$. (*a*) Time-averaged energy spectrum. (*b*) Time series of vorticity kurtosis (solid curve) and stream-function kurtosis (dashed curve) from a statistically steady portion of the run. (*c*) Time-averaged spectral energy flux, $\epsilon(k)$. (*d*) The Kolmogorov constant $C_2(k) = k^{\frac{5}{3}}E(k)\epsilon(k)^{-\frac{2}{3}}$. The average value of C_2 is 5.8.

In contrast to the simulations of the enstrophy range, the value of C_2 seems to be, at most, weakly dependent on forcing and dissipation parameters. We also find C_2 to be independent of numerical resolution, at least for $k_{\max} = 128$ and $k_{\max} = 256$. The values we find (between 5.5 and 6.5) are more or less consistent with closure-model predictions by Kraichnan (1971) ($C_2 = 6.69$), and with numerical simulations by Lilly (1972) ($C_2 \approx 6$). In more recent simulations, Herring & McWilliams (1985) have found $C_2 \leqslant 4.8$ in a manner similar in the way we found $C_2 = 5.8$, and Frisch & Sulem (1984) found $C_2 \approx 9$ by using a least-squares fit to the spectrum and average fluxes. (We obtain $C_2 = 8$ using the latter method.) However, the present study has much greater inertial-range resolution than any of the aforesaid direct numerical simulations.

5.2 *Anisotropic flows*

When the β-effect is added to flows forced at high wavenumbers, the changes in behaviour are similar to those seen with forcing at low wavenumbers. The three flow regimes described in §4 are seen, with the first transition occurring in the vicinity of $k_\beta = 1$. In this case, however, the vorticity kurtosis remains significantly greater than

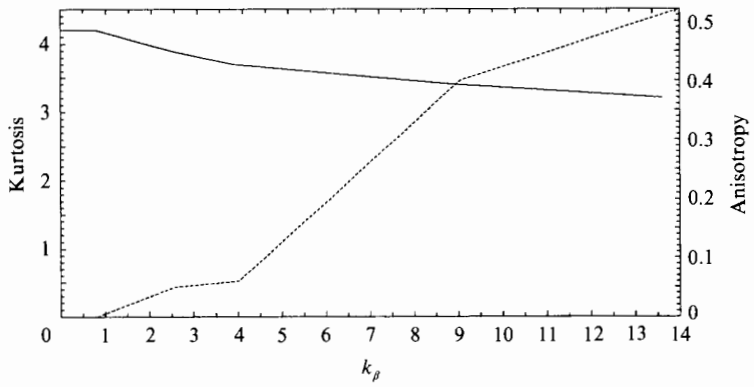

FIGURE 9. Average vorticity kurtosis (solid curve) and the average anisotropy (dashed curve) as functions of k_β from simulations forced in the range $80 \leqslant k \leqslant 84$ with low-wavenumber dissipation acting for $k \leqslant 20$.

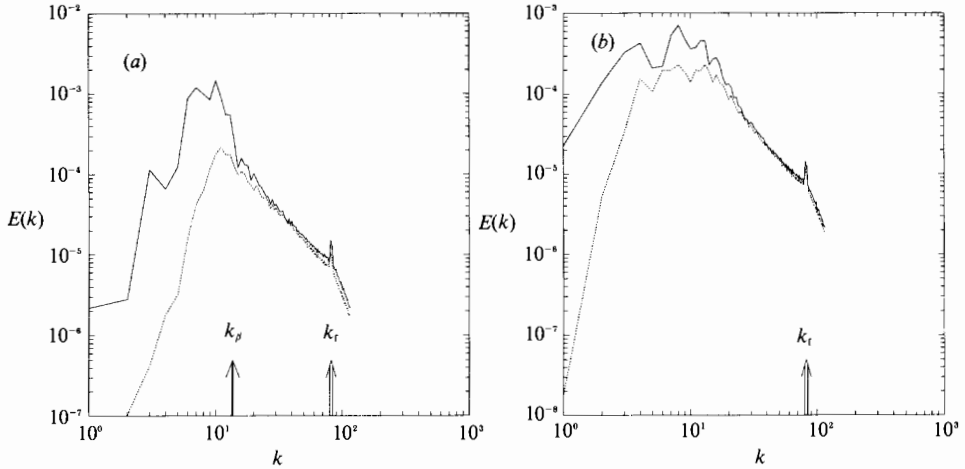

FIGURE 10. Energy spectra of zonal motions (solid curve) and meridional motions (dashed curve) from simulations forced in the range $80 \leqslant k \leqslant 84$. (*a*) True β-effect with $k_\beta = 13.6$. (*b*) Anisotropic forcing with $\beta \neq 0$ for $k \leqslant 20$. Otherwise, this case uses the same parameters as in (*a*).

3 even when the anisotropy is high, but it does decrease steadily as k_β increases (figure 9). This difference leads to a slightly more elaborate interpretation of the boundaries between the flow regimes. The anisotropy increases when k_β approaches the energy peak in the spectrum. On the other hand, the vorticity kurtosis reaches a value of 3 as k_β approaches the enstrophy peak (which is approximately coincident with the forcing range). For flows forced at relatively low wavenumbers, the energy and enstrophy peaks are approximately the same, so high anisotropy coincides with near-Gaussian vorticity kurtosis. For simulations forced at high wavenumbers, the energy peak remains at low wavenumbers, while the enstrophy peak is at high wavenumbers, explaining the presence of significantly non-Gaussian kurtosis accompanied by high anisotropy.

As long as k_β is chosen to be small enough so that the inertial range can still be resolved (e.g. $k_\beta \leqslant 20$), the slope of the inertial-range spectrum remains approximately proportional to $k^{-\frac{5}{3}}$, and the value of the constant C_2 is essentially unchanged. The inverse cascade of energy is effectively arrested at k_β, where energy accumulates.

Without explicitly introducing frictional processes (a non-zero α in (2.5)) energy continues to accumulate at this scale. This would actually cause the value of k_β to fall until it lies within a low-wavenumber frictional subrange, whence equilibration can occur.

The anisotropy of the flow is largely manifest at those wavenumbers smaller than k_β (figure 10*b*). However, in some contrast to the simulations forced at low wavenumbers, the anisotropy is much smaller in the energy inertial range than in the enstrophy range and even seems to approach zero at intermediate wavenumbers. We may again introduce anisotropic forcing to the system by allowing the β-effect to be non-zero only at low wavenumbers to investigate the transfer of anisotropy through the energy inertial range. Figure 10(*a*) shows a simulation identical to the one shown in figure 10(*b*), except that β is zero for $k > 20$. Significant anisotropy is seen only at those wavenumbers where β enters the dynamics directly, implying that anisotropy is rather inefficiently transferred against the reverse energy cascade.

6. Forcing at high and low wavenumbers

Observations of the energy spectrum of the Earth's atmosphere have revealed the existence of two well-defined spectral slopes at relatively large scales (Nastrom & Gage 1985). An enstrophy range with a slope of approximately k^{-3} driven by baroclinic instability is seen in the synoptic scales from about 600 to 3000 km. At the mesoscales ranging from a few to approximately 200 km, a possible energy range driven by smaller-scale convection is seen with a slope very close to $k^{-\frac{5}{3}}$. Larsen, Kelley & Gage (1982) postulate the need for a continuous sink of energy and enstrophy to dispose of a possible buildup in the transition region between the two inertial ranges. On the other hand, closure-model calculations by Lilly (1989) have shown the coexistence of both inertial ranges without the need for dissipation. In this section we investigate whether a stable coexistence of two inertial ranges is possible in direct numerical simulations of two-dimensional turbulence.

Figure 11 shows the results of a simulation forced for $10 \leqslant k \leqslant 14$ and for $160 \leqslant k \leqslant 165$. Both forcings are given the same correlation time, but the amplitude is five times greater for the high-wavenumber range. Although the lower-wavenumber inertial range is not particularly well resolved, the higher range ($40 < k < 160$) is well resolved and the energy spectrum has a slope of approximately $-\frac{5}{3}$. The Kolmogorov constant C_2 found in this range agrees with the value found for forcing at high wavenumbers only. The lower-wavenumber range has a slope steeper than k^{-3}, and coherent structures are seen in the vorticity field (figure 1*f*) (plate 1), just as in the simulations forced only at low wavenumbers. The energy and enstrophy fluxes are seen to be constant through most of the region between the forcing ranges (figure 11*b*). In particular the constant upscale energy transfer continues through the steeply sloping 'enstrophy' inertial range, and the enstrophy cascades down through the shallow 'energy' inertial range. Dissipation is active only for $k \leqslant 5$ and $k \geqslant 200$, so a sink is not present and not needed in the transition region between the two spectral slopes.

In Lilly's calculations, the transition from enstrophy to energy inertial-range slopes occurs approximately at a wavenumber defined as

$$k_0 \equiv (\eta/\epsilon)^{\frac{1}{2}}, \tag{6.1}$$

where η and ϵ are the enstrophy and energy cascade rates, respectively, both taken positive. Aside from the phenomenological closure calculations Lilly gives, this

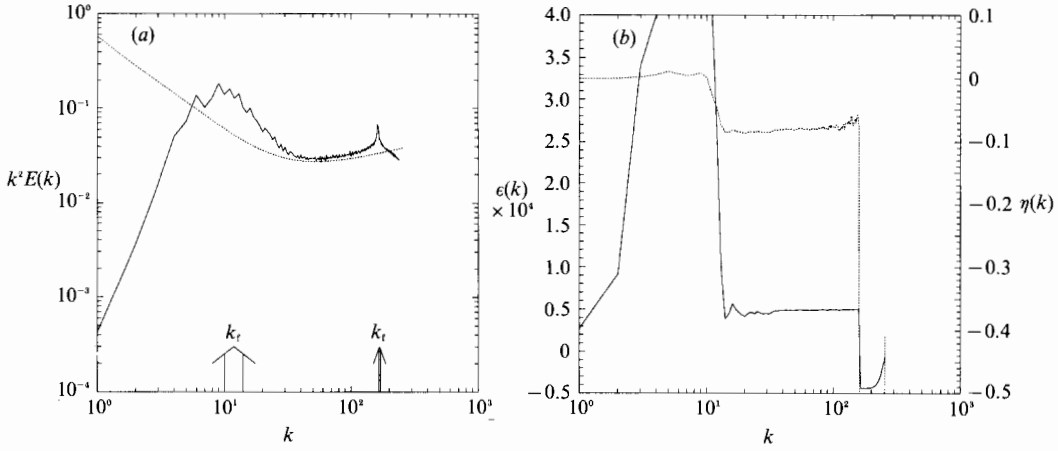

FIGURE 11. Flow diagnostics from a simulation forced in two distinct wavenumber ranges: $10 \leqslant k \leqslant 14$ and $160 \leqslant k \leqslant 165$. (*a*) Time-averaged enstrophy spectrum. The dashed line indicates the spectral shape predicted by Leith's (1968) closure as demonstrated by Lilly (1989). (*b*) Time-averaged spectral energy flux $\epsilon(k)$ (solid curve) and enstrophy flux $\eta(k)$ (dashed curve).

scaling wavenumber arrives simply from equating the energy and enstrophy inertial-range expressions (3.1) and (5.1), to within an constant factor. In our simulation, we find $k_0 \approx 40$, which is roughly in accord with the location of the change in spectral slope (figure 11*a*). We can also compare our spectrum with Lilly's result based on Leith's (1968) diffusive closure model,

$$E(k) = [(\epsilon k^{-\frac{5}{2}} + \eta k^{-\frac{9}{2}})/2B]^{\frac{2}{3}}, \tag{6.2}$$

where B is a constant. The transition range in the spectrum from our simulation appears to be more abrupt than the gentle change in curvature of the closure spectrum (shown as the dashed line in figure 11*a*), but the general shape between the forcing ranges are in good agreement, especially in the $k^{-\frac{5}{3}}$ range. However, in the light of our previous discussion about the inapplicability of k^{-3} inertial-range expressions, any disagreement in the lower range may be moot since the closure predicts k^{-3} for $k \ll k_0$. In any case it is quite remarkable that downscale enstrophy transfers and upscale energy transfers can simultaneously coexist over the same wavenumbers, with identically zero dissipation.

The coexistence of inertial ranges is not affected by the addition of the β-effect, though the position of the transition wavenumber k_0 may vary. As in the simulations forced only at low wavenumbers, there is large anisotropy in the smaller-wavenumber range. In contrast to the simulations forced only at high wavenumbers, there is also significant anisotropy in the approximately $k^{-\frac{5}{3}}$ range, possibly carried there by the non-zero enstrophy cascade that now exists in this range.

7. Discussion

In this study we have been concerned with the energy spectra of the enstrophy and energy inertial ranges in two-dimensional turbulence, the roles of coherent vortices and Rossby wave radiation, and the possible non-universality of the enstrophy range. In particular, it is often implicitly assumed that coherent vortices in forced–dissipative two-dimensional turbulence are the cause of spectral slopes steeper than the k^{-3} inertial-range prediction. In this study, we have introduced

various mechanisms – Rossby wave radiation, friction – that exert a destructive influence on the vortices, and examined the energy spectra that result.

When the β-effect was added to a system containing coherent vortices and with a steep spectrum, the vortices were readily destroyed by radiation of Rossby waves for sufficiently large k_β. Often a shallower spectral slope, although still steeper than k^{-3}, ensued; typically, the energy spectra were seen to equilibrate in a range between $k^{-3.3}$ and $k^{-3.5}$. If the spectrum was already k^{-3} before the introduction of β (say because of the nature of the low-wavenumber forcing and dissipation), then the β-effect serves merely to inhibit enstrophy transfer to high wavenumbers (effectively by inhibiting energy transfer to low wavenumbers) and hence steepens the spectrum which again equilibrates around $k^{-3.4}$. Thus, although the spectra with β are typically not as steep as those with coherent vortices, the -3 range is still not easily recovered.

Finding that the β-effect can shallow the spectrum apparently contradicts Rhines' (1975) result that the addition of β tends to steepen the slope owing to inhibition of turbulent transfers. There are some important differences in these cases. Rhines reached his conclusion by considering an initial-value problem. However, analysis of initial tendencies of the flow as performed by Rhines are not obviously relevant to our statistically steady case. Second, the presence of coherent structures in our simulations inhibits turbulent transfers by removing a significant fraction of the vorticity from the active cascade. This effect is evidently more efficient in inhibiting the enstrophy transfer and steepening the slope than is the similar effect of β. When β is weak, the effect of the vortices is seen and the slope is steep; when β is strong enough to destroy vortices the inhibition of the enstrophy cascade by β is less than the inhibition by the vortices, and the slope is shallower.

One should not conclude solely on the basis of two-dimensional or geostrophic turbulence arguments, that the energy spectrum of a true geophysical fluid (for example the Earth's atmosphere) should have a slope of exactly k^{-3}, even for those scales that are expected to behave quasi-geostrophically. For not only do flows with coherent vortices have steep slopes, but so do many flows with significant β-effect. Only for a system dominated by dissipation and having minimal β-effect might we expect an approximately k^{-3} spectrum, a rather narrow parameter regime unlikely to be achieved in most geophysical flows. Furthermore, the range of scales over which the atmosphere behaves quasi-two-dimensionally is not significantly greater than the simulations presented herein. Thus, one cannot argue that because the atmosphere's 'resolution' is higher than any numerical model it will still yield a k^{-3} spectrum, because at small scales the atmosphere behaves three-dimensionally. However, there is some evidence for an enstrophy cascade and a k^{-3} energy spectrum (Boer & Shepherd 1983; Nastrom & Gage 1985) in the atmosphere. Whether this is coincidental, or is due to some other physical process producing a scale-independent turnover time, remains unknown at this time.

Phenomenologically, the inertial-range scalings in both two and three dimensions are obtained by assuming that energy or enstrophy transfer is spectrally local, in the sense that the energy cascade through a particular wavenumber depends only on the energy spectrum at that wavenumber, and not on the mechanisms of forcing or dissipation. For a $k^{-\frac{5}{3}}$ energy spectrum this assumption is *a posteriori* satisfied (Kraichnan 1971). However, a strict k^{-3} spectrum is non-local and almost self-inconsistent, since for a straining rate at wavenumber k given by

$$R_k = \left\{ \int_0^k p^2 E(p)\, \mathrm{d}p \right\}^{\frac{1}{2}}, \tag{7.1}$$

the contributions of each octave to the integrand are all equal for a -3 spectrum, implying non-locality. Using an eddy turnover time based on (7.1) leads of course to the log-corrected range. However, as soon as locality has been dropped, that spectrum becomes but one of many phenomenological possibilities, along with the intermittency-corrected spectra of Basdevant *et al.* (1981), rather than a result demanded of scaling. Now, for a spectrum shallower than -3, for example $-\frac{5}{3}$, the contributions are dominated by wavenumbers at the upper end of the integral, close to k, and locality is more assured. This suggests that a -3 spectrum is close to the shallowest slope which is likely to be generally achieved for the enstrophy range: any shallower spectra will have more local enstrophy transfers, and hence satisfy the Kolmogorovian assumptions, but will then be disallowed by Kolmogorovian scaling arguments. However, a steeper spectrum may well have non-local enstrophy transfer and violate the locality assumption; the scaling arguments then simply do not apply and a steep spectrum is not inconsistent. In this sense -3 spectra are not robust and form, rather, a shallowest limit on the slope.

When approximate k^{-3} spectra do arise, we find that the 'constant' C_1 appearing in the inertial-range theories (3.1) does not appear to be universal if a local measure for the eddy turnover time is used. However, a slightly more general formulation of the inertial-range arguments leads to the recovery of universality, at least for the cases we have tested. It implies that the k^{-3} spectra arise from the small scales behaving like a passive scalar, with the local strain rate (7.1) completely dominated by the forcing scale.

Nonlocality is prevalent in the simulations yielding steeper spectra. In our simulations the presence of coherent structures is always associated with the spectrum being steeper than the classical prediction, although whether coherent structures 'cause' the steep spectra and the non-locality, or whether they are simply a consequence of non-locality, has not been clarified. Non-locality may be interpreted physically as a relatively large-scale vortex straining much smaller scales as if it were a mean shear, an interpretation which seems to apply to anisotropic flows as well. Simulations that are forced to be anisotropic at large scales appear to transfer their anisotropy directly to small scales by straining out long filaments with a preferred orientation. However, phenomenological theories of intermittent two-dimensional turbulence (e.g. Basdevant *et al.* 1981) do caution against interpretation of non-local straining as implying non-localness of enstrophy transfer, since the 'active' spectrum will always be shallower than k^{-3}.

The reverse energy cascade, on the other hand, is much more robust in its agreement with classical inertial-range theory. We find that the constant C_2 defined by inertial-range theories (5.1) is largely independent of model forcing parameters. The introduction of the β-effect does not change the inertial-range behaviour for $k > k_\beta$, and the resulting anisotropy is seen to remain mostly at wavenumbers smaller than k_β. While we have found that the energy spectrum for the inverse cascade of energy to large scales is close to $k^{-\frac{5}{3}}$, the mechanism behind this cascade is still somewhat unclear. It is often supposed that energy is transferred upscale by small vortices coalescing into larger vortices. We do not see direct evidence supporting this, since most of the vortices in these simulations are seen at scales that are of the order of the forcing scale and smaller, and not larger. This does not necessarily imply that this process is unimportant, since some mergers are undoubtedly occurring, resulting in vortices of slightly larger scale. It is of course possible that such mergers produce motions of larger scale that simply are not recognizable as vortices in maps of the vorticity field.

Finally, we presented simulations of two-dimensional turbulence with forcing at two different scales. An inverse energy cascade to low wavenumbers, and an enstrophy cascade to high wavenumbers, can coexist over the same range of wavenumbers with a fairly distinct change in slope within, coinciding roughly with the scaling wavenumber (6.1). No dissipation is needed in intermediate wavenumbers in order to achieve equilibration. The simultaneous existence of these ranges, with apparently quite different dynamics, serves only to emphasize our limited understanding of the precise mechanisms of energy and enstrophy transfer in the inertial ranges.

We would like to thank T. Warn, J. McWilliams, D. Lilly, B. Legras, G. Holloway and J. Herring for helpful conversation, correspondence, and input. This work was funded by NSF (ATM 8914004), ONR (N00014-90-J-1618) and IGPP/Los Alamos. Some of the calculations presented here were performed at the San Diego Supercomputer Center.

REFERENCES

BABIANO, A., BASDEVANT, C., LEGRAS, B. & SADOURNY, R. 1987 Vorticity and passive-scalar dynamics in two-dimensional turbulence. *J. Fluid Mech.* **183**, 379–397.

BASDEVANT, C., LEGRAS, B., SADOURNY, R. & BELAND, M. 1981 A study of barotropic model flows: intermittency, waves and predictability. *J. Atmos. Sci.* **38**, 2305–2326.

BATCHELOR, G. K. 1969 Computation of the energy spectrum in two-dimensional turbulence. *Phys. Fluids Suppl.* **12**, II 233–239.

BENZI, R., PALADIN, G., PATARNELLO, P., SANTANGELO, P. & VULPIANI, A. 1986 Intermittency and coherent structures in two-dimensional turbulence. *J. Phys.* A: *Math. Gen.* **19**, 3771–3784.

BOER, G. J. & SHEPHERD, T. G. 1983 Large scale two-dimensional turbulence in the atmosphere. *J. Atmos. Sci.* **40**, 164–184.

FORNBERG, B. 1977 A numerical study of 2D turbulence. *J. Comput. Phys.* **25**, 1–31.

FRISCH, U. & SULEM, P.-L. 1984 Numerical simulation of the inverse cascade in two-dimensional turbulence. *Phys. Fluids* **27**, 1921–1923.

GRANT, H. L., STEWART, R. W. & MOILLET, A. 1962 Turbulence spectra from a tidal channel. *J. Fluid Mech.* **12**, 241–268.

HERRING, J. R. 1975 Theory of two-dimensional anisotropic turbulence. *J. Atmos. Sci.* **32**, 2254–2271.

HERRING, J. R. & MCWILLIAMS, J. C. 1985 Comparison of direct numerical simulation of two-dimensional turbulence with two-point closure: the effects of intermittency. *J. Fluid Mech.* **153**, 229–242.

HOLLOWAY, G. 1984 Contrary roles of planetary wave propagation in atmospheric predictability. In *Proc. La Jolla Inst. Workshop on Predictability of Fluid Flows* (ed. G. Holloway & B. West), pp. 593–600.

HOLLOWAY, G. & HENDERSHOTT, M. 1977 Stochastic closure for nonlinear Rossby waves. *J. Fluid Mech.* **82**, 747–765.

HOLLOWAY, G. & KRISTMANNSSON, S. 1984 Stirring and transport of tracer fields by geostrophic turbulence. *J. Fluid Mech.* **141**, 27–50.

KOLMOGOROV, A. N. 1941 The local structure of turbulence in incompressible fluid at very high Reynolds number. *Dokl. Acad. Sci. USSR.* **30**, 299–303.

KOLMOGOROV, A. N. 1962 A refinement of previous hypotheses concerning the local structure of turbulence in a viscous incompressible fluid at high Reynolds number. *J. Fluid Mech.* **13**, 82–85.

KRAICHNAN, R. H. 1967 Inertial ranges in two-dimensional turbulence. *Phys. Fluids* **10**, 1417–1423.

KRAICHNAN, R. H. 1971 Inertial-range transfer in two- and three-dimensional turbulence. *J. Fluid Mech.* **47**, 525–535.

LARSEN, M. F., KELLEY, M. C. & GAGE, K. S. 1982 Turbulence spectra in the upper troposphere and lower stratosphere at periods between 2 hours and 40 days. *J. Atmos. Sci.* **39**, 1035–1041.

LEGRAS, B., SANTANGELO, P. & BENZI, R. 1988 High resolution numerical experiments for forced two-dimensional turbulence. *Europhys. Lett.* **5**, 37–42.

LEITH, C. E. 1968 Diffusion approximation for two-dimensional turbulence. *Phys. Fluids* **11**, 671–673.

LEITH, C. E. & KRAICHNAN, R. H. 1972 Predictability of turbulent flows. *J. Atmos. Sci.* **29**, 1041.

LESIEUR, M. & HERRING, J. 1985 Diffusion of a passive scalar in two-dimensional turbulence. *J. Fluid. Mech.* **161**, 77–95.

LILLY, D. K. 1972 Numerical simulation studies of two-dimensional turbulence: Part 1. Models of statistically steady turbulence. *Geophys. Fluid Dyn.* **3**, 290–319.

LILLY, D. K. 1989 Two-dimensional turbulence generated by energy sources at two scales. *J. Atmos. Sci.* **46**, 2026–2030.

MCWILLIAMS, J. C. 1984 The emergence of coherent vortices in turbulent flow. *J. Fluid Mech.* **146**, 21–43.

NASTROM, G. D. & GAGE, K. S. 1985 A climatology of atmospheric wavenumber spectra of wind and temperature observed by commercial aircraft. *J. Atmos. Sci.* **42**, 950–960.

PATTERSON, G. S. & ORSZAG, S. A. 1971 Spectral calculation of isotropic turbulence: efficient removal of aliasing interaction. *Phys. Fluids* **14**, 2538–2541.

RHINES, P. B. 1975 Waves and turbulence on the β-plane. *J. Fluid Mech.* **69**, 417–443.

SADOURNY, R. & BASDEVANT, C. 1985 Parameterization of subgrid-scale barotropic and baroclinic eddies in quasi-geostrophic models: Anticipated potential vorticity method. *J. Atmos. Sci.* **42**, 1353–1363.

SALMON, R. 1982 Geostrophic turbulence. In *Topics in Ocean Physics, Proc. Intl Schaol Phys. 'Enrico Fermi', Varenna, Italy*, pp. 30–78.

SANTANGELO, P., BENZI, R. & LEGRAS, B. 1989 The generation of vortices in high resolution, two-dimensional decaying turbulence and the influence of initial conditions on the breaking of self-similarity. *Phys. Fluids* A **1**, 1027–1034.

SMAGORINSKY, J. 1963 General circulation experiments with the primitive equations. *Mon. Weath. Rev.* **91** (3), 99–164.

VALLIS, G. K. 1985 Remarks on the predictability of two- and three-dimensional flow. *Q. J. Met. Soc.* **111**, 1039–1047.

VALLIS, G. K. & HUA, B. 1988 Eddy viscosity of the anticipated potential vorticity method. *J. Atmos. Sci.* **45**, 617–627.

YAKHOT, V. & ORSZAG, S. 1986 Renormalization group analysis of turbulence. 1. Basic theory. *J. Sci. Comput.* **1**, 3–51.